Energy Engineering

Tech Science Press

Doi:10.32604/ee.2025.065753

ARTICLE

Research on Optimal Scheduling of Integrated Energy Systems with Wind-Photovoltaic-Biogas-Storage Considering Carbon Capture Systems and Power-to-Gas Coordination

Yunfei Xu[1], Jianfeng Liu[1,*], Tianxing Sun[1], Heran Kang[1] and Xiaoqing Hao[2]

[1]Economic and Technological Research Institute, State Grid Inner Mongolia Eastern Electric Power Co., Ltd., Hohhot, 010020, China
[2]Inner Mongolia Hengsheng New Energy Technology Co., Ltd., Baotou, 014030, China

*Corresponding Author: Jianfeng Liu. Email: liujianfeng0314@163.com

Received: 21 March 2025; Accepted: 16 May 2025; Published: 24 July 2025

ABSTRACT: In order to promote the utilization level of new energy resources for local and efficient consumption, this paper introduces the biogas (BG) fermentation technology into the integrated energy system (IES). This initiative is to study the collaborative and optimal scheduling of IES with wind power (WP), photovoltaic (PV), and BG, while integrating carbon capture system (CCS) and power-to-gas (P2G) system. Firstly, the framework of collaborative operation of IES for BG-CCS-P2G is constructed. Secondly, the flexible scheduling resources of the source and load sides are fully exploited, and the collaborative operation mode of CCS-P2G is proposed to establish a model of IES with WP, PV, and BG multi-energy flow coupling. Then, with the objective of minimizing the intra-day operating cost and the constraints of system energy balance and equipment operating limits, the IES with WP, PV, and BG collaborative optimal scheduling model is established. Finally, taking into account the uncertainty of the output of WP and PV generation, the proposed optimal scheduling model is solved by CPLEX, and its validity is verified by setting several scenarios. The results show that the proposed collaborative operation mode and optimal scheduling model can realize the efficient, low-carbon, and economic operation of the IES with WP, PV, and BG and significantly enhance the utilization of new energy for local consumption.

KEYWORDS: Integrated energy system; biogas; power-to-gas; carbon capture system; collaborative

1 Introduction

With the increasing depletion of fossil energy and the frequent natural disasters caused by the greenhouse effect, clean and efficient energy conversion and utilization have become an important development direction and the main way of change in the global energy field [1]. The proposal of China's "carbon peaking and carbon neutrality" target promotes the transformation of energy and a low-carbon economy. It also puts forward the important initiative of building a new modern energy system by developing and consuming new energy according to local conditions [2]. Although the WP, PV, and other clean energy research technologies tend to mature, the development of new energy is facing multiple challenges, such as large-scale development, efficient local consumption, and the need to ensure a safe and reliable supply of electricity. In this context, multi-energy complementary IES is the key platform for connecting energy supply and demand. It can realize the coupling and joint supply of multiple energy sources through rational and optimal dispatching and distribution of heterogeneous energy sources, improve the comprehensive utilization efficiency of energy, and effectively enhance the capacity of renewable energy consumption and the reliability of energy supply.

IES contains power, gas, heat, and other energy structures that can be coordinated and optimized through the energy conversion devices, storage facilities, and other equipment formed by the production, supply, and distribution of integrated systems. IES is an important way to realize the goal of the "carbon peaking and carbon neutrality" strategy, which has become a hot research topic for researchers.

P2G technology provides a new way of energy conversion and spatial-temporal transfer. This technology solves the problem of renewable energy accommodation and realizes peak cutting and valley filling of power load by converting WP, PV, or other energy into natural gas, which is easy to be stored [3]. At present, P2G is widely used to power and gas coupled energy systems to improve WP and PV accommodation and the flexibility of system operation. In [4], the authors proposed a joint application of P2G and combined heat and power (CHP) units in IES. The superiority of energy utilization efficiency is verified through simulation. In [5], the authors proposed a model for coordinated optimization of micro gas turbine (GT) and P2G systems. This model supplies natural gas to micro GT through the P2G system, which not only reduced the carbon emissions but also reduced the natural gas procurement cost of the system. In [6], the authors established a model of peak cutting and valley filling considering P2G, which improved the economy of the whole system operation. In [7], the authors provided an in-depth analysis of the conversion process of P2G technology, including aspects of the electrolytic tank model, system steady state, and transient models. In summary, the application of P2G devices to IES has significant practical engineering value and significance.

Carbon capture power plants (CCPP) are transformed from coal-fired and gas-fired power plants through the CCS, which can significantly reduce the level of carbon emissions. By controlling the energy consumption of CCS, CCPP are characterized by flexible operation and fast response. Compared to conventional power plants, CCPP can realize low-carbon and economic dispatch operation of IES [8]. In [9], the authors introduced CCS to a WP generation system. Its example simulations showed that the CCS can reduce the impact of WP fluctuations on the system. A system model of P2G-CCS is constructed, which utilizes CO_2 captured by CCPP as feedstock to supply the P2G. This model can save the material cost and reduce the carbon emission at the same time [10,11]. In [12], the authors established a collaborative model of CCS and P2G. The conclusion showed that the collaborative operation of CCS and P2G can effectively promote the accommodation of WP and realize the recycling of carbon. In [13], the authors applied CCS technology and P2G technology to the scheduling model of IES. In [14], the authors proposed a collaborative operation model of liquid storage CCS-P2G-CHP, and the system's economy and low-carbon benefit were improved by executing the optimal scheduling possible while taking the cost of carbon transactions into account. The current research on P2G-CCPP mainly focuses on electricity-gas systems, rarely involves the IES of electricity, gas, and heat, and does not realize the coordinated and optimized scheduling among multiple energy sources of electricity, gas, and heat.

Current research on BG utilization is also developing rapidly under the guidance of China's national policy, especially in rural or suburban areas with abundant biomass resources. Biomass energy in these areas is easy to connect to the IES, which is an important direction for future energy development. In [15], the authors established a BG-WP-PV IES model based on an energy hub (EH). Then, the BG storage tank was introduced to participate in the optimal scheduling of electricity, heat, and gas systems, which reduced the operation cost of the system. In [16], the authors analyzed the economic and environmental benefits of hybrid power generation technology with renewable energy such as BG, WP, and PV, which reduces CO_2 emissions. In [17], the authors considered the uncertainty of environmental factors such as WP and PV in remote mountainous areas and established a micro-energy network model of BG-WP-PV to model the heat load of buildings in detail, which improved the economy and reliability of the system's energy supply. In [18], the authors added BG to IES containing renewable energy sources such as WP and PV, which proved that BG can save fuel costs instead of traditional diesel. In [19], the authors designed a cooperative

renewable energy scheduling system using BG-PV-WP to increase the penetration of renewable energy sources and lower the system's running costs. In [20], the authors adopted the concept of an EH to represent the coupling relationship among energy sources. Then, an optimal scheduling model of IES containing BG-WP-PV is established. And its calculation results show that low-carbon and economic operation of the IES can be achieved through optimal dispatching. In [21], the authors constructed an interval optimization model for an integrated rural energy system with hydrogen production from biogas fermentation electrolysis in order to solve the problems of low biomass utilization, wind power uncertainty, and intermittency in rural winter. In [22], the authors developed a two-tier optimization model for a biogas-IES considering the thermal comfort of heating customers and natural gas price fluctuations and resolved the uncertainty of the probabilistic results using an improved Latin hypercube sampling method. In [23], a day-ahead optimal scheduling model for an IES is proposed, which takes into account the coupling of biomass and P2G to reduce carbon emissions during the operation of an industrial park. Currently, IES containing BG have begun to receive attention. However, the research on multi-energy coupling systems that integrate the consideration of BG-WP-PV, P2G, CCS, and energy storage has not been reported.

For this reason, this thesis introduces biogas into the electricity-heat-gas IES and constructs a WP-PV-BG IES considering CCS and P2G conversion in order to realize the efficient local consumption and utilization of renewable energy, which has good research significance and practical value. The main contributions of this paper include:

(1) A grid-connected WP-PV-BG integrated energy microgrid composed of multiple renewable energy sources is proposed to utilize the complementary characteristics among PV, WP, and BG to realize the synergistic operation of BG-CCS-P2G in a low-carbon economy while promoting the virtuous cycle of the ecosystem.
(2) Aiming at the stochastic uncertainty of WP and PV in the WP-PV-BG IES, scenario generation of WP and PV output following the probability distribution constraints is generated by the Latin hypercube sampling technique. The stochastic uncertainty problem is transformed into a deterministic problem for collaborative optimization computation by using the scenario abatement technique and combining it with the characteristics of the maximum probability distribution.
(3) A collaborative optimal scheduling model of WP-PV-BG IES considering CCS and P2G is established, and four typical cases are set to verify the feasibility and superiority of the constructed WP-PV-BG IES.

The main structure of this paper: Section 1 constructs the IES architecture and completes the modeling. Section 2 constructs the optimal scheduling model, including the objective function, constraint conditions, and solving algorithm. Section 3 verifies the feasibility of the scheduling model developed in this paper through an arithmetic example analysis. The conclusion is drawn in Section 4.

2 Structure and Model Construction of the IES with WP-PV-BG

This paper proposes an IES structure of WP-PV-BG proposed with P2G and CCS (Fig. 1). The system includes the external energy supply, the multiple energy storage, the energy conversion, and the load. The system realizes the comprehensive utilization of energy and meets the load demand flexibly through the coupling of three energy sources: electricity, heat, and gas. External energy supply includes a variety of energy sources such as PV, WP, BG, the external power grid, and the external gas grid. Energy storage includes electric energy storage, thermal storage, and gas storage to achieve a balance between supply and demand. Energy conversion equipment includes P2G, CCS, and BG to reduce carbon emissions through rational utilization of biomass. In addition, GT and electric boilers (EB) are used as energy supply equipment to provide electricity and heat energy for the system.

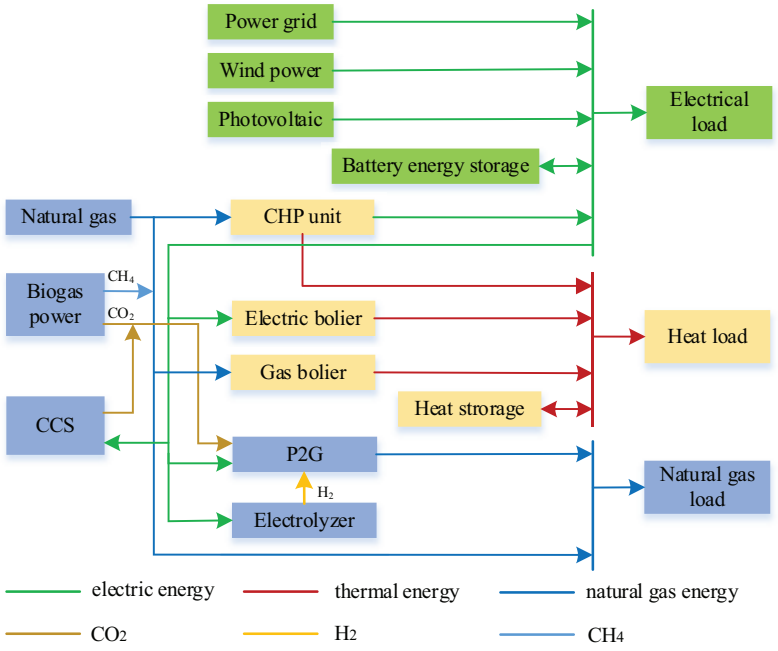

Figure 1: Structure of IES

2.1 BG Fermentation System

As a greenhouse gas, CH_4 has a serious impact on climate change. By collecting and utilizing methane from agricultural waste (such as BG digesters), direct emissions of these greenhouse gases into the atmosphere can be effectively reduced. At the same time, BG, as a clean fuel, its combustion releases far fewer pollutants than traditional fossil fuels (such as coal, oil, and natural gas), which helps to improve air quality. Fig. 2 shows the process of BG production.

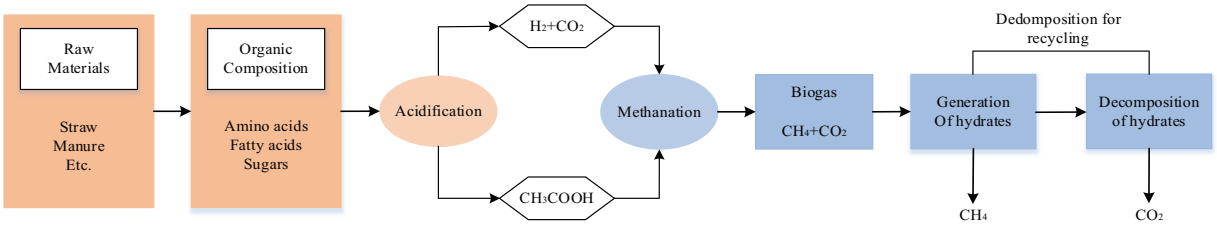

Figure 2: Working principle of BG digester

As can be seen in Fig. 2, the fermentation stage of BG includes hydrolysis, acidification, formation of acetic acid, and methanation. Then BG composed of CH_4 and CO_2 is obtained. BG is purified by the hydrate method. Because the pressure of a hydrate formation of CO_2 is lower than that of CH_4, CO_2 forms hydrate into a hydrate phase at a certain temperature and pressure. CH_4 is enriched in the gas phase, realizing the separation of CH_4 and CO_2. By decomposing the gas hydrate containing CO_2, the high-purity CO_2 gas can be recovered and the decomposed aqueous solution can be recycled. The CH_4 in BG can be supplied to CHP, while CO_2 is used by P2G to produce gas.

2.2 CCS-P2G-BG Collaborative Operation Framework

Fig. 3 shows the CCS-P2G-BG collaborative operation framework. The BG produced from the digester is separated into CH_4 and CO_2. CH_4 is directly used as a fuel for CHP, and CO_2 can be used as a feedstock for P2G to synthesize CH_4. Next, CCS can capture CHP and CO_2 emitted from BG digesters. P2G uses surplus renewable energy to convert CO_2 separated from the BG digester and CO_2 captured by CCS into CH_4 gas for gas equipment to use, which improves energy efficiency and reduces carbon emissions of the system.

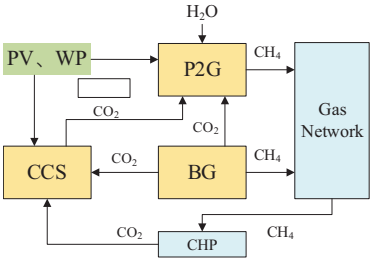

Figure 3: Working schematic diagram of P2G-CCS-BG coupling system

2.3 CCS-P2G-BG Coupling Model

2.3.1 BG Modeling

The digester reacts to produce CO_2 and CH_4. Temperature is an important environmental factor affecting BG production, which are proportional to the calorific value of the BG, and the correlation formula is as follows:

$$Q_{bio,t}^{BT} = f_{bio}\left(T_{\text{out}} - T_0\right)^2 + Q_{max,t}^{BT} \tag{1}$$

$$Q_{bio,t}^{BT} = Q_{CH_4,t}^{BT} + Q_{CO_2,t}^{BT} \tag{2}$$

$$Q_{CH_4,t}^{BT} = \lambda^{BT} Q_{bio,t}^{BT} \tag{3}$$

$$Q_{CO_2,t}^{BT} = \left(1 - \lambda^{BT}\right) Q_{bio,t}^{BT} \tag{4}$$

where $Q_{bio,t}^{BT}$ represents the gas production capacity of the BG digester, m^3; f_{bio} represents the temperature coefficient of BG digester, $m^3/°C$; T_{out} represents the operating temperature of BG digester, °C; T_0 is the optimal fermentation temperature of the BG digester, °C; $Q_{max,t}^{BT}$ is the maximum gas production of the BG digester, m^3; $Q_{CH_4,t}^{BT}$ represents the amount of CH_4 produced by the BG digester, m^3; $Q_{CO_2,t}^{BT}$ represents the amount of CO_2 produced by the BG digester; λ^{BT} represents the CH_4 conversion rate of the BG digester.

2.3.2 CCS Modeling

The amount of CO_2 captured by CCS is related to the CO_2 emitted by the fuel as follows:

$$Q_{CO_2,t}^{CCS} = \eta^{CCS} Q_{CO_2,t}^{pai} \tag{5}$$

$$Q_{CO_2,t}^{XCCS} = (1 - \eta^{CCS}) Q_{CO_2,t}^{pai} \tag{6}$$

Moreover, the power consumption of CCS is related to the amount of CO_2 captured, and the specific relationship is as follows:

$$P_{e,t}^{CCS} = P_{fix,t}^{CCS} + P_{cap,t}^{CCS} \tag{7}$$

$$P_{cap,t}^{CCS} = \lambda^{CCS} Q_{CO_2,t}^{CCS} \tag{8}$$

where $Q_{CO_2,t}^{CCS}$ represents the amount of CO_2 captured by the CCS for CHP unit emissions; $Q_{CO_2,t}^{pai}$ represents the amount of CO_2 emitted by the fossil fuel unit during period t; η^{CCS} represents capture efficiency for CCS systems; $Q_{CO_2,t}^{XCCS}$ represents the amount of CO_2 not captured by CCS and emitted to the atmosphere at time t; $P_{e,t}^{CCS}$, $P_{fix,t}^{CCS}$ and $P_{cap,t}^{CCS}$ represent operational energy consumption, fixed energy consumption and capture energy consumption of the CCS structure, respectively; λ^{CCS} represents the CCS energy consumption factor.

2.3.3 P2G Modeling

Due to the complexity of the internal nature of P2G, the current literature usually simplifies P2G to an energy conversion model with fixed efficiency. It acts as an active load bus on the electrical load side and as a gas source node on the gas side. The P2G model is represented as follows:

$$Q_{H_2,t}^{EL} = \frac{\eta^{EL} P_{e,t}^{EL}}{H_{H_2}} \tag{9}$$

where $Q_{H_2,t}^{EL}$ represents the amount of CH_4 produced at time t; $P_{e,t}^{EL}$ represents the electrical power consumed by P2G at time t; η^{EL} represents the conversion efficiency of P2G; H_{H_2} represents the calorific value of CH_4.

2.3.4 Modeling of CCS and P2G Coupling

CO_2 captured by CCS is mainly synthesized into methane and sequestered in the following relationship:

$$Q_{CO_2,t}^{CCS} = Q_{CO_2,t}^{ME} + Q_{CO_2,t}^{STO} \tag{10}$$

where $Q_{CO_2,t}^{CCS}$ is the amount of CO_2 captured by CCS from CHP unit, part of which is used for methane reaction and part of which is used for storage; $Q_{CO_2,t}^{ME}$ represents the amount of CO_2 used to synthesize CH_4; $Q_{CO_2,t}^{STO}$ represents the amount of stored CO_2.

Molar mass relationship for the synthesis of CH_4 from H_2 produced by P2G and CO_2:

$$Q_{CH_4,t}^{ME} = \frac{1}{4} Q_{H_2,t}^{EL} \tag{11}$$

$$Q_{CH_4,t}^{ME} = \left(Q_{CO_2,t}^{ME} + Q_{CO_2,t}^{BT}\right) \frac{1}{1000 V_m} \tag{12}$$

where $Q_{CH_4,t}^{ME}$ represents the molar mass of the synthesized CH_4; V_m represents the molar volume of the gas in the standard state.

3 Optimal Operation Model

3.1 Objective Function

The optimized scheduling objective of IES proposed in this paper is to minimize the total operating cost of the system with the following objective function:

$$F = min\left\{f_w + f_q + f_c + f_g + f_b\right\} \tag{13}$$

where f_w represents the system operation and maintenance cost; f_q represents the WP and PV abandonment penalty cost; f_c represents the CO_2 related cost; f_g represents the comprehensive energy purchase cost; f_b represents the BG digester capacity cost.

3.1.1 Operation and Maintenance Cost

$$f_w = \sum_{t=1}^{T}\left(\sum_{i\in\Omega} C_{on}^{i} u_t^i \left(1-u_{t-1}^i\right) + \sum_{i\in\Omega} C_{off}^{i} u_{t-1}^i \left(1-u_t^i\right) + \sum_{i\in\Omega} C_w^i P_t^i\right)$$
$$\Omega = \{EB, GB, CHP, ES, BG, P2G, CCS\} \tag{14}$$

where Ω denotes each unit; T represents the day-ahead system scheduling time, which is 24 h; C_{on}^{i}, C_{off}^{i} and C_w^i represent the start, stop and maintenance cost of each unit, respectively; u_t^i represents the operating status of each unit, which is a binary variable. When the unit is running, $u_t^i = 1$, and when the unit is shut down, $u_t^i = 0$; P_t^i represents the output power of the unit at time t.

3.1.2 Cost of WP and PV

$$f_q = \sum_{t=1}^{T} C^{pen}\left(P_{curt,t}^{WP} + P_{curt,t}^{PV}\right) \tag{15}$$

where C^{pen} represents the renewable energy reduction penalty factor; $P_{curt,t}^{WP}$ and $P_{curt,t}^{PV}$ represent the WP and PV power reduction, respectively.

3.1.3 CO_2 Related Cost

$$f_c = \sum_{t=1}^{T}\left(r_{em}\left[Q_{CO_2,t}^{XCCS} - Q_{em}\right] + r_{sto} Q_{CO_2,t}^{STO}\right) \tag{16}$$

where r_{em} represents the excess carbon emission factor; Q_{em} represents the standard CO_2 emission allowance; r_{sto} represents the cost factor for storing CO_2.

3.1.4 Comprehensive Energy Purchase Cost

$$f_g = \sum_{t=1}^{T}\left(r_{e,t} P_{e,t}^{buy} + r_{g,t} Q_{g,t}^{buy}\right) \tag{17}$$

where $r_{e,t}$ and $r_{g,t}$ represent the real-time electricity and gas prices, respectively; $P_{e,t}^{buy}$ and $Q_{g,t}^{buy}$ represent the amount of electricity and gas purchased from the external market in time t of the system, respectively.

3.1.5 BG Digester Raw Material Cost

$$f_b = r_{bio,t} Q_{bio,t}^{BT} \tag{18}$$

where $r_{bio,t}$ represents the cost factor of gas production in the digester.

3.2 Constraints

3.2.1 CHP Unit Constraints

The CHP unit constraints are described by Eq. (19).

$$\begin{cases} P_{e,t}^{CHP} \le P_{e,max}^{CHP} - k_1 P_{h,t}^{CHP} \\ P_{e,t}^{CHP} \ge P_{e,min}^{CHP} - k_2 P_{h,t}^{CHP} \\ P_{e,t}^{CHP} \ge k_3 P_{h,t}^{CHP} \\ P_{e,t}^{CHP} + \eta^{CHP} P_{h,t}^{CHP} = H_{CH4} Q_{g,t}^{CHP} / (1000 V_m) \end{cases} \tag{19}$$

where $P_{e,t}^{CHP}$ represents the output electric power of the CHP unit at time t; $P_{h,t}^{CHP}$ represents the output heat power of the CHP unit at time t; $P_{e,max}^{CHP}$ and $P_{e,min}^{CHP}$ represent the maximum and minimum output electric power of the CHP unit, respectively; k_1, k_2 and k_3 represent the operating parameters of the CHP unit, respectively; η^{CHP} represents the CHP conversion rate of the CHP unit; H_{CH4} represents the calorific value of natural gas; $Q_{g,t}^{CHP}$ represents the volume of natural gas consumed by the CHP unit at time t; V_m represents the molar volume of gas in the standard condition.

3.2.2 GB Constraint

The GB operation constraint is represented by Eq. (20).

$$P_{h,t}^{GB} = \eta^{GB} Q_{g,t}^{GB} H_{CH_4} \tag{20}$$

where $P_{h,t}^{GB}$ represents the heat power output of GB at time t; $Q_{g,t}^{GB}$ represents the natural gas consumption of GB at time t; η^{GB} represents the conversion efficiency of GB; H_{CH_4} represents the calorific value of natural gas.

3.2.3 EB Constraint

The constraint of EB is represented by Eq. (21).

$$P_{h,t}^{EB} = \eta^{EB} P_{e,t}^{EB} \tag{21}$$

where $P_{h,t}^{EB}$ represents the heat power output of the EB at time t; $P_{e,t}^{EB}$ represents the electric power consumed by the EB at time t; η^{EB} represents the energy conversion efficiency.

3.2.4 Electric ES Constraint

The electric ES constraints are represented by Eq. (22).

$$\begin{cases} E_{e,t}^{EES} = (1 - \gamma^{EES}) E_{e,t-1}^{EES} + \eta_{ch}^{EES} P_{ch,t}^{EES} - \frac{1}{\eta_{dis}^{EES}} P_{dis,t}^{EES} \\ E_{e,min}^{EES} \le E_{e,t}^{EES} \le E_{e,max}^{EES} \\ P_{ch,min}^{EES} \le P_{ch,t}^{EES} \le P_{ch,max}^{EES} \\ P_{dis,min}^{EES} \le P_{dis,t}^{EES} \le P_{dis,max}^{EES} \\ P_{ch,t}^{EES} \cdot P_{dis,t}^{EES} = 0 \\ S_{e,t_0}^{EES} = S_{e,T}^{EES} \end{cases} \tag{22}$$

where $E_{e,t}^{EES}$ represents the energy storage capacity of the electric energy storage device at time t; γ^{EES} represents the energy consumption coefficient of the electric energy storage device; η_{ch}^{EES} and η_{dis}^{EES} represent the charging and discharging efficiency, respectively; $P_{ch,t}^{EES}$ and $P_{dis,t}^{EES}$ represent the charging and discharging power of the electric energy storage device at time t, respectively; $E_{e,max}^{EES}$ and $E_{e,min}^{EES}$ represent the upper and

lower limits of the electric energy storage capacity, respectively; $P_{ch,max}^{EES}$ and $P_{ch,min}^{EES}$ represent the upper and lower limits of the charging power, respectively; $P_{dis,max}^{EES}$ and $P_{dis,min}^{EES}$ represent the upper and lower limits of the discharging power, respectively; S_{e,t_0}^{EES} and $S_{e,T}^{EES}$ represent the electric energy storage capacity at the beginning and end of the time, respectively.

3.2.5 Heat ES Constraints

The heat ES constraint is similar to the electric ES constraints.

3.2.6 Renewable Energy Unit Constraints

Renewable energy units include WP and PV, and their constraints are as follows:

$$\begin{cases} P_{av,t}^{WP} = P_{e,t}^{WP} + P_{curt,t}^{WP} \\ P_{av,t}^{PV} = P_{e,t}^{PV} + P_{curt,t}^{PV} \end{cases} \tag{23}$$

where $P_{av,t}^{WP}$ and $P_{av,t}^{PV}$ represents the available WP and PV in time t, respectively; $P_{e,t}^{WP}$ and $P_{e,t}^{PV}$ represent the actual power output of WP and PV in time t, respectively; $P_{curt,t}^{WP}$ and $P_{curt,t}^{PV}$ represent the power reduction of WP and PV in time t, respectively.

3.2.7 Power Balance Constraints

$$\begin{cases} P_{e,t}^{WP} + P_{e,t}^{PV} + P_{e,t}^{CHP} + P_{e,t}^{buy} + P_{dis,t}^{EES} = P_{e,t}^{sell} + P_{e,t}^{EL} + P_{e,t}^{CCS} + P_{e,t}^{EB} + P_{ch,t}^{EES} + P_{\mathrm{e},t}^{L} \\ P_{h,t}^{CHP} + P_{h,t}^{buy} + P_{h,t}^{GB} + P_{h,t}^{EB} = P_{h,t}^{L} + P_{h,t}^{sell} \\ Q_{CH_4,t}^{BL} + Q_{g,t}^{buy} + Q_{CH_4,t}^{ME} = Q_{g,t}^{sell} + Q_{g,t}^{CHP} + Q_{g,t}^{GB} + Q_{g,t}^{L} \end{cases} \tag{24}$$

where $P_{e,t}^{sell}$, $P_{h,t}^{sell}$ and $Q_{g,t}^{sell}$ represent the electricity, heat and gas energy sold to the external market in time t of the system, respectively; $P_{\mathrm{e},t}^{L}$, $P_{h,t}^{L}$ and $Q_{g,t}^{L}$ represent the electricity, heat and gas loads of the system in time t, respectively; $Q_{g,t}^{CHP}$ and $Q_{g,t}^{GB}$ represent the amounts of CH_4 consumed by the CHP units and hot GBs in time t, respectively.

3.2.8 Upper and Lower Limits of Unit Output Power Constraints

$$u_t^i P_{\min}^i \le P_t^i \le u_t^i P_{\max}^i, i \in \{P2G, EB, GB, CHP\} \tag{25}$$

where $P_{\max}^i$ and $P_{\min}^i$ represent the maximum and minimum output power of the unit, respectively.

3.2.9 Unit Climbing Constraints

$$P_{rd,\max}^i \le P_t^i - P_{t-1}^i \le P_{ru,\max}^i, i \in \{P2G, EB, GB, CHP\} \tag{26}$$

where $P_{ru,\max}^i$ and $P_{rd,\max}^i$ represent the maximum upward and downward climbing power of the unit, respectively.

3.2.10 Unit Start-Stop Constraints

In order to avoid damage to equipment caused by frequent start-ups and shutdowns, it is necessary to limit the starting and stopping time of the unit. Eq. (27) ensures that the start-up time and downtime of IES component are not lower than its minimum value. Eq. (28) limits the power of the unit during start-up and

downtime to no less than the minimum power, ensures that the unit can provide sufficient power during operation and shutdown, and avoids damage to the equipment during low-power operation.

$$\begin{cases} \left(T^i_{on,t} - T^i_{on,\min}\right)\left(u^i_{t+1} - u^i_t\right) \geq 0 \\ \left(T^i_{off,t} - T^i_{off,\min}\right)\left(u^i_t - u^i_{t+1}\right) \geq 0 \\ \begin{cases} u^i_t = 1, u^i_{t+1} = 0; \\ u^i_{t-1} = 0, u^i_t = 1; \\ P^i_t = P^i_{\min} \end{cases} \end{cases} \tag{27}$$

$$i \in \Omega_{CHP} \cup \Omega_{EB} \cup \Omega_{GB} \cup \Omega_{BT} \cup \Omega_{P2G} \cup \Omega_{CCS} \tag{28}$$

where $T^i_{on,t}$ and $T^i_{off,t}$ represent the start and stop times of the unit, respectively; $T^i_{on,\min}$ and $T^i_{off,\min}$ represent minimum start and stop time of the unit, respectively; $P^i_{\min}$ represents minimum power for start and stop of the unit.

3.2.11 BG, P2G and CCS Operation Constraints

$$0 \leq Q_{zq} \leq f_{bio,t} \times Q^{BT}_h \tag{29}$$

where Q_{zq} represents the amount of BG utilized.

3.2.12 Input Power Limit and Climbing Power Limit for P2G Devices

$$u^{EL}_{e,t} P^{EL}_{\min} \leq P^{EL}_{e,t} \leq u^{EL}_{e,t} P^{EL}_{\max} \tag{30}$$

$$\Delta P^{EL}_{rd,\max} \leq P^{EL}_{e,t} - P^{EL}_{e,t-1} \leq \Delta P^{EL}_{ru,\max} \tag{31}$$

where $P^{EL}_{\min}$ and $P^{EL}_{\max}$ are the minimum and maximum limits of P2G power consumption, respectively; $\Delta P^{EL}_{rd,\max}$ and $\Delta P^{EL}_{ru,\max}$ are the maximum ramp up and down rates of P2G power consumption.

3.2.13 CCS Output Constraints

$$P^{CCS}_{\min} \leq P^{CCS}_{e,t} \leq P^{CCS}_{\max} \tag{32}$$

where $P^{CCS}_{\min}$ and $P^{CCS}_{\max}$ represent maximum and minimum power consumption of CCS, respectively.

3.3 Solving Method

In this paper, a low-carbon economic dispatch model of IES considering CCS cooperative WP, PV, hydrogen, BG and storage is constructed. The nonlinear model is transformed into a mixed integer linear programming (MILP) model by piecewise linear. The CPLEX solver in the YALMIP toolbox was invoked in MATLAB to perform simulation solutions, so as to determine the output of the energy supply equipment and the energy conversion equipment in each time period, thus realizing the economic and low-carbon operation

of IES. The standard form for solving the model is as follows:

$$\begin{cases} \min c^T x \\ \quad s.t. \quad A_{ineq} x \le b_{ineq} \\ \qquad\quad A_{eq} x = b_{eq} \\ \qquad\quad x_{\min} \le x_i \le x_{\max}, \quad i \in I \\ \qquad\quad x_j \in \{0,1\}, \qquad\quad j \in J \end{cases} \tag{33}$$

where the optimization variable x includes the output of the energy supply equipment, the input of the conversion equipment, the input and output of the energy storage device, as well as the purchase of electricity and gas from the power grid and gas grid. $A_{eq}x = b_{eq}$ is an equality constraint that includes the energy balance equation of the system and the balance equation of the energy storage device. $A_{ineq}x \le b_{ineq}$ is an inequality constraint that includes output constraints for each device in the system.

4 Example Analysis

4.1 Renewable Energy Uncertainty Processing

Multiple random scenarios of wind power and photovoltaic output following probability distribution constraints are generated by Latin hypercube sampling technique. The scene reduction method based on Kantorovich distance is used to reduce these scenes, so as to simulate the uncertainty of WP and PV output.

4.1.1 Renewable Energy Probability Model

In this paper, the normal distribution is used to describe the prediction error of PV and WP:

$$\begin{cases} F(PV) = \frac{1}{\sqrt{2\pi}\sigma_{PV}} \exp\left[-\frac{(P_V-\mu_{PV})^2}{2\sigma_{PV}^2}\right] \\ F(PW) = \frac{1}{\sqrt{2\pi}\sigma_{PW}} \exp\left[-\frac{(P_W-\mu_{PW})^2}{2\sigma_{PW}^2}\right] \end{cases} \tag{34}$$

where σ_{PV}, σ_{PW} present the standard deviations of PV and WP; μ_{PV}, μ_{PW} present the expectations of *PV and WP*.

4.1.2 Latin Hypercube Sampling Generation Scenario

In this paper, the sampling scale is set to 1000 and the steps of using Latin hypercube sampling to generate photovoltaic multi-scenario output are as follows:

(1) The distribution curve of *F(PV)* is divided into 1000 intervals, and the spacing is 1/1000.

(2) Take a number in each of the 1000 intervals, and set the sampling point of the *x*th interval as *Nx*, then the cumulative probability of *Nx* is:

$$P_x = (1/1000)\, r_x + (x-1)/1000 \tag{35}$$

where P_x presents the cumulative probability of sampling point x; r_x presents any number in the interval [0~1].

(3) The sampling value K_x of each interval can be obtained by bringing P_x back to the distribution function:

$$K_x = F_{PV}^{-1}(P_x) \tag{36}$$

(4) Repeat the operation of step 3 to obtain 1000 sampling values of PV, generate a 1 × 1000-dimensional matrix, and randomly sort into 1000 scenarios.

4.1.3 Scenario Reduction

Based on the above 1000 randomly generated scenes, set the number of scenes after reduction to 5, and the reduction process is as follows:

(1) Initially, the probability of each scene is 1/1000 and the initial number of scenes is $n = 1000$;
(2) Calculate the Kantorovich distance $D_x(Si, Sj)$ for each scene:

$$D_x\left(s_i, s_j\right) = \left[\sum_{s=1}^{s}\left(L_{i,t} - L_{j,t}\right)^2\right]^{\frac{1}{2}} \tag{37}$$

(3) The closest scene y within the range of scene x is selected, and the probability and the product of the Kantorovich distances of the two scenes are set equal:

$$P_x D_x\left(s_i, s_j\right) = P_y D_y\left(s_i, s_j\right) \tag{38}$$

(4) Repeat step 3 to select the scene z with minimum $P_x D_x(S_i, S_j)$ and delete it, then update the number of scenes to $n = n - 1$, at which point the probability of scene y is updated to $P_y = P_y + P_z$;
(5) Repeat steps 2–4 until $n = 5$ and the scene cut ends.

The scenario generation and reduction process for wind power is the same as above. Fig. 4 shows the clustering cut results of wind power and PV output scenarios, in which the probabilities of scenarios 1 to 5 are 0.422, 0.113, 0.172, 0.138, and 0.155, respectively, and scenario 1 with the highest probability is selected as the final scenario of the predicted output of PV and WP.

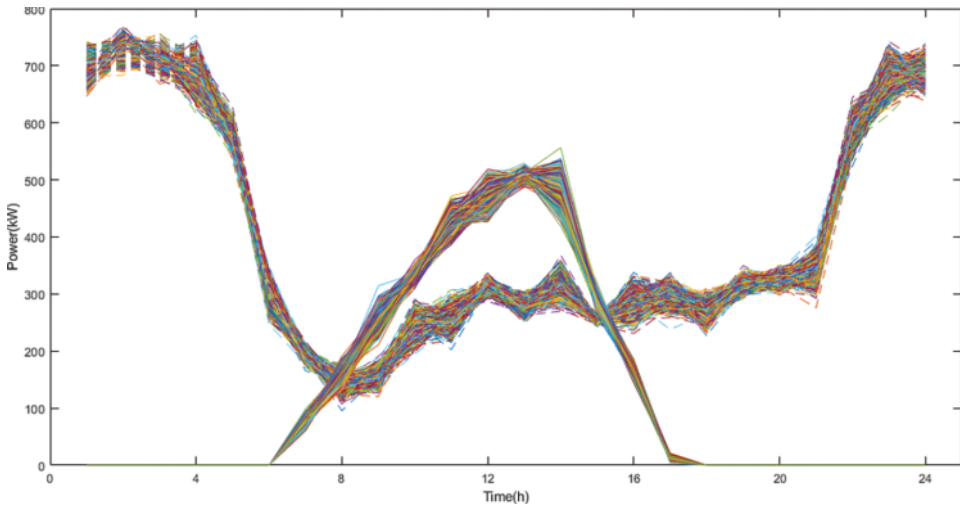

(a)

Figure 4: (Continued)

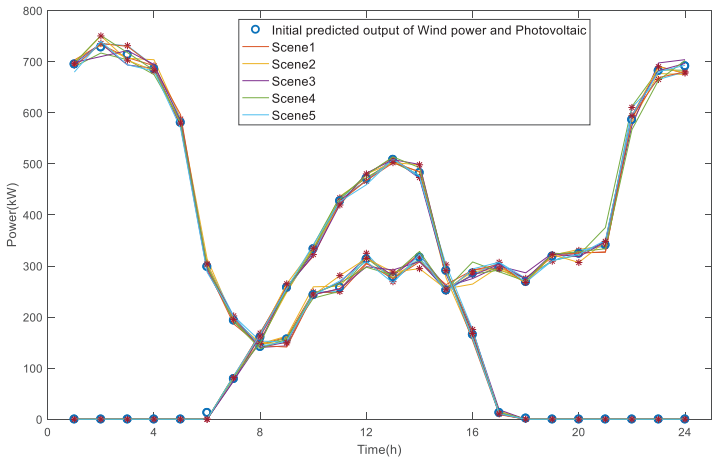

(b)

Figure 4: Scenario clustering reduction results; **(a)** 1000 PV and WP generation scenarios; **(b)** Typical output scenarios of PV and WP

4.2 System Parameters and Scene Settings

In order to verify the economy and effectiveness of the IES operation proposed in this paper, the DES structure given in Fig. 1 is used as an example for simulation calculation. The forecast curve of electric, gas and heat load forecast curves, as well as the day-ahead predicted output power of WP and PV are shown in Fig. 5, where *Pwav* is the WP output; *Pvav* is the PV output; Pl is the active load; Ql is the reactive load; and Hl is the heat load. The real-time prices of electrical, heat and gas energy are seen in Table 1. The relevant parameter data is seen in Table 2.

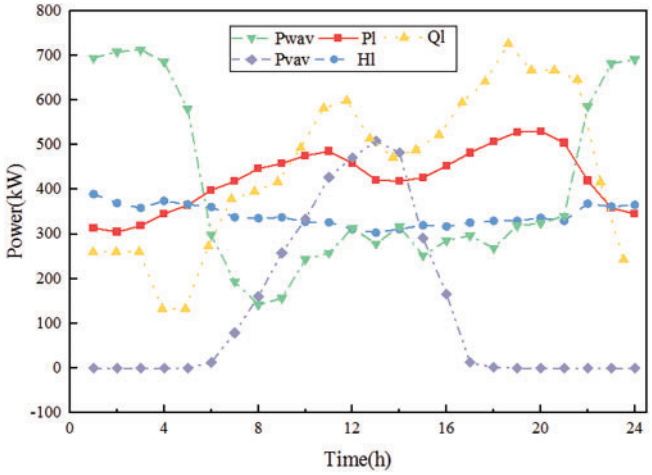

Figure 5: Predicted output of WP, PV, and load

Table 1: Hourly energy price

Energy types	Time	Value
Electrical (yuan/kWh)	1:00–6:00	0.35
	7:00–8:00, 12:00–14:00, 19:00–24:00	0.50
	9:00–11:00, 15:00–18:00	0.65
Gas (yuan/m^3)	1:00–6:00, 20:00–24:00	3.61
	9:00–10:00, 13:00–16:00	4.83
	7:00–8:00, 11:00–12:00, 17:00–19:00	8.46
Thermal (yuan/kWh)	1:00–24:00	0.4

Table 2: Unit parameters

Unit	Parameter	Value	Unit	Parameter	Value
CHP	$P_{\max}$ (kW)	400	BT	$P_{\max}$ (m^3)	20
	$P_{\min}$ (kW)	100		E^{BT} (m^3)	200
	k_1	0.4		f_{bio}	1
	k_2	0.4		λ^{BT}	0.7
	k_3	0.8		r_{bio}	0.1
	η^{CHP}	0.9	P2G	$P_{\max}$ (kW)	150
GB	$P_{\max}$ (kW)	200		$P_{\min}$ (kW)	0
	$P_{\min}$ (kW)	50		η^{EL}	0.85
	η^{GB}	0.9	CCS	$P_{\max}$ (kW)	10
EB	$P_{\max}$ (kW)	100		$P_{\min}$ (kW)	0
	$P_{\min}$ (kW)	0		η^{CCS}	0.8
	η^{EB}	0.95		λ^{CCS}	1.97
TES	E^{TES}	500	EES	E^{EES}	500
	η^{TES}	0.95		η^{EES}	0.99

Four scenarios are set up to calculate the operating costs through co-optimization used to verify the feasibility and superiority of the carbon capture and power-to-gas wind swamp IES proposed in this thesis. Among them, Case 1: Optimized scheduling of IES day-ahead without considering P2G, CCS, and BG digester. Case 2: IES day-ahead optimal scheduling with only P2G considered on the base case. Case 3: Consider the day-ahead optimal scheduling of IES of P2G and CCS. Case 4: IES day-ahead optimal scheduling considering both P2G and CCS as well as BG digester.

4.3 Cost Analysis

Optimization calculations are performed for the four cases set up, and the results are shown in Table 3.

Table 3: The total cost of IES in cases 1–4

Cost category	Case 1	Case 2	Case 3	Case 4
IES operation and maintenance costs: f_w	286.53	373.97	417.26	428.07
IES punishment cost of abandoning wind and light: f_q	1012.33	181.17	10.16	0.00

(Continued)

Table 3 (continued)

Cost category		Case 1	Case 2	Case 3	Case 4
System CO_2-related costs: f_c	IES carbon capture costs	0.00	0.00	143.59	140.55
	IES carbon emissions cost	235.20	239.38	−28.39	−27.90
	IES carbon sequestration costs	0.00	0.00	48.46	62.87
	IES carbon purchase cost	0.00	494.55	0.00	0.00
IES comprehensive energy purchase costs: f_g	IES power purchase costs	0.00	0.00	0.00	0.00
	IES heat purchase costs	41.80	354.89	360.19	459.28
	IES gas purchase costs	21,622.47	19,029.86	19,815.57	19,588.50
IES total costs: F		23,198.32	20,673.82	20,766.85	20,651.37

From Table 3, it can be seen that Case 1 has the highest wind abandonment cost of RMB 1012.33, indicating insufficient renewable energy consumption. And after the introduction of the power-to-gas device, the renewable energy of Cases 2, 3, and 4 is substantially consumed, especially Case 4 realizes 100% of the renewable energy accommodation. Cases 1 and 2 cause large CO_2 emissions due to the non-existence of CCS, and the cost of carbon emissions amounted to RMB 235.2 and RMB 239.38, respectively. In contrast, cases 3 and 4 would benefit from the carbon trading market, with carbon trading gains of RMB 28.39 and RMB 27.90, respectively. Although a BG digester was added to Case 4, the CO_2 separated from the BG digester was not fully utilized due to multiple factors such as wind and light storage, resulting in a larger CO_2-related cost than Case 3. While Case 2 also has a higher CO_2-related cost because it is not able to obtain CO_2 from the system itself and needs to purchase CO_2 from the external carbon market to satisfy the operation of P2G.

In all four cases, there is no need to buy electricity from an external energy network, because it is self-sufficient. Cases 2, 3 and 4 are all equipped with P2G, which can improve the self-supplying capacity of gas. However, because P2G is a high energy-consuming equipment, the electric energy output of CHP is increased, thus the heat energy output is reduced. For this reason, Cases 2, 3, and 4 all require the purchase of thermal energy, resulting in an increase in the cost of purchasing heat compared to Case 1 by RMB 313.09, RMB 318.39, and RMB 417.48, respectively. From the perspective of total cost, Case 4, which also considers P2G, CCS, and BG digester, has the lowest cost of RMB 20,651.37, which is 10.98% lower relative to Case 1, and realizes low-carbon economic operation.

4.4 Analysis of the Level of Renewable Energy Accommodation

The process of renewable energy accommodation is analyzed through four cases, as shown in Fig. 6 *Pwav* denotes the WP output; *Pvav* denotes the PV output; *Pwav* + *Pvav* denotes the sum of the WP and PV outputs, which is the set point; Cases 1–4 is the sum of the WP and PV grid-connected power, which is the WP and PV power that can be accepted by IES after the optimal dispatch, that is, the grid-connected power.

From Fig. 6, it is evident that there are substantial WP outputs during the time intervals of 1:00 to 5:00, 22:00 to 24:00, and 10:00 to 13:00. During this period, Case 1 cannot be consumed resulting in an increase in WP abandonment cost. For Case 2, which considers P2G, most of the renewable energy is consumed, but there is still the problem of insufficient accommodation. Case 3 considers both P2G and CCS, and the level of renewable energy accommodation increases significantly. Case 4 considers a BG digester in addition to Case 3, and realizes 100% of renewable energy accommodation.

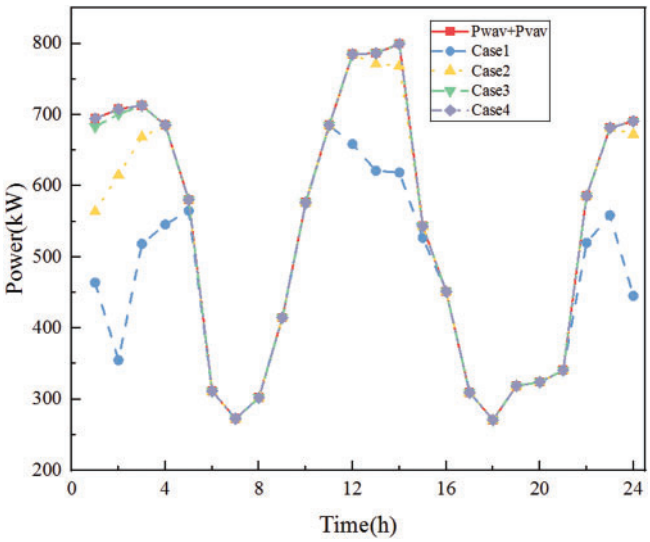

Figure 6: Renewable energy consumption levels under different cases

4.5 Analysis of Carbon Emission Levels

Fig. 7 shows the CO_2 emissions of the system under the four cases. From the figure, it can be seen that the emissions of Case 2 are larger than those of Case 1, which is due to the fact that the WP and PV renewable energy outputs are lower in the 5:00 to 7:00 and 19:00 to 22:00 time periods. In order to meet the normal operation of the P2G, the output of the CHP unit in Case 2 is increased, which leads to an increase in the CO_2 emissions. For Cases 3 and 4, where CCS is considered, the carbon emissions are significantly reduced and the carbon emission curves are approximately the same. The operation of the BG system does not have a significant impact on the level of carbon emissions from the system, which is generally consistent with Case 3.

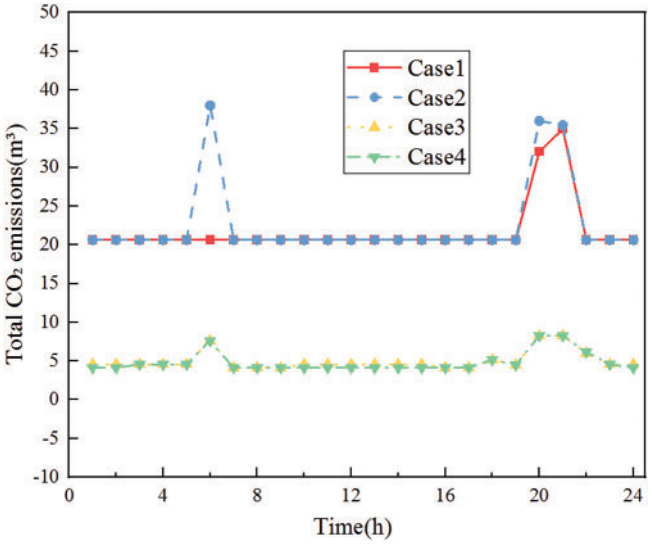

Figure 7: System CO_2 emissions under different cases

4.6 Analysis of Scheduling Results

Because case 4 has the lowest total operating cost, this section only analyzes the output of each running device in case 4.

Fig. 8 shows the electric energy scheduling results, where *Peesch* denotes the charging power of the battery; *Peb* denotes the electricity consumption of EB; *Pccs* denotes the power of the CCS; *Pel* denotes the power of the electrolytic tank; *Psell* denotes the power of the electricity sold to the system; *Peesids* denotes the battery discharge power; *Pchp* denotes the power of CHP unit; *Pw* denotes the wind turbine power; *Pv* denotes the PV power, and *Pbuy* denotes the power of the electricity purchased from the system.

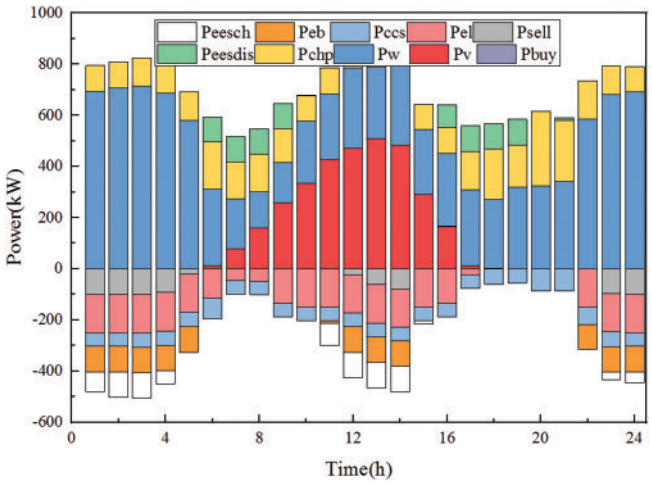

Figure 8: Electricity scheduling results

From Fig. 8, the devices store electricity during periods of abundant WP and PV resources from 1:00 to 4:00, 11:00 to 14:00, and 23:00 to 24:00. They discharge stored energy during periods of low WP and PV resources from 6:00 to 9:00 and 16:00 to 19:00, which plays the role of peak-shaving and valley-filling in renewable energy dispatch. Likewise, the CHP unit also boosts their output to meet the electrical load during low renewable energy output hours. EB converts electricity to heat to meet the system's heat energy demand during periods of high renewable energy output. P2G converts surplus electricity into gas for efficient energy use. CCS equipment is kept in operation to capture CO_2 from CHP and BG digesters.

Fig. 9 shows the results of heat energy scheduling, where *Hsell* denotes the amount of heat sold to the system; *Htesch* denotes the amount of heat stored in the heat storage tank; Heb denotes the value of heat produced by the EB; *Hzq* denotes the amount of heat produced by the BG digester; *Hchp* denotes the amount of heat produced by CHP unit; *Htesdis* denotes the amount of heat discharged from the heat storage tank; and Hgb denotes the amount of heat produced by the GB. As seen in Fig. 10, the heat storage unit stores heat energy during the low-demand period from 11:00 to 14:00 and provides heat to the system during periods of insufficient CHP output from 7:00 to 9:00 and 17:00 to 19:00. In addition to meeting the heat load demand, the system needs to purchase heat from the external energy market when the EB and the CHP output is insufficient.

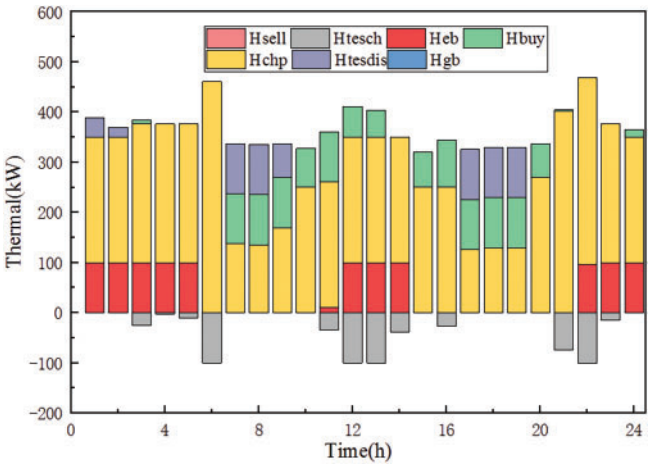

Figure 9: Heat energy scheduling results

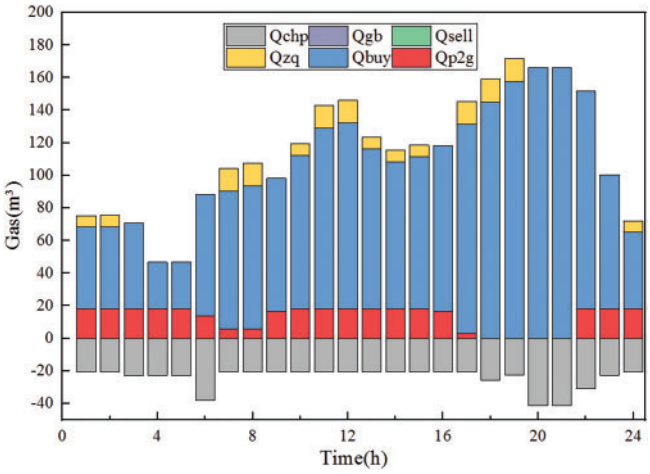

Figure 10: Natural gas scheduling results

Fig. 10 shows the gas dispatch results, where *Qchp* denotes the gas consumption of the CHP unit; *Qgb* denotes the gas consumption of GB, *Qsell* denotes the gas sold to the system, *Qzq* denotes the gas production from BG; *Qbuy* denotes the gas purchased from the system; *Qp2g* denotes the gas produced by P2G. As can be seen from Fig. 11, P2G and BG digester can provide gas to the system during the operation of the system. The shortage of gas meets the load demand by purchasing gas from gas companies. Equipment that consumes gas includes CHP and GB.

In summary, the system maintains the balance between supply and demand through different energy conversions and coordinated operation of units. The P2G unit converts CO_2 into CH_4 for use by the gas unit when there is surplus electricity. The addition of BG also shares a small part of the supply pressure for the system, and the BG digester supply is mainly affected by the real-time gas transaction price, providing gas during higher price hours to reduce the purchase of gas in the system. Similarly, gas from P2G can also compensate for part of the gas demand, thereby reducing the cost of gas purchase. All units and equipment in the system operate cooperatively to achieve low-carbon economic operation of the system.

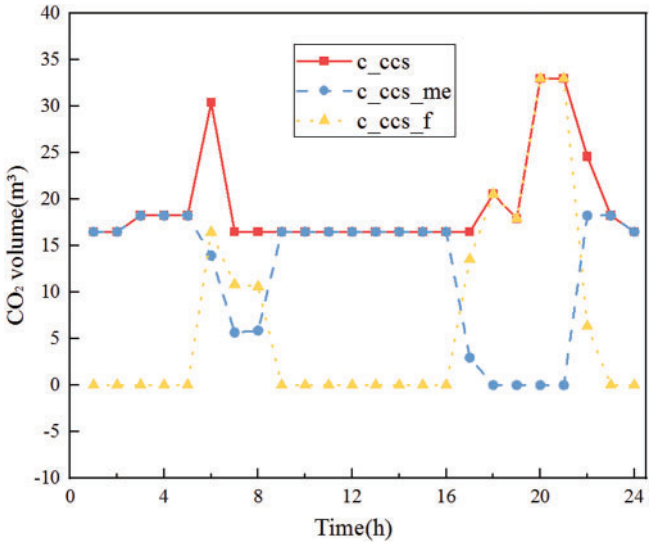

Figure 11: Carbon capture device CO_2 traces in case 4

4.7 Carbon Trace Analysis

Fig. 11 shows the CO_2 traces captured by the CCS in Case 4, where c_ccs denotes the amount of CO_2 captured by CCS; c_ccs_me denotes the amount of CO_2 utilized by P2G; and c_ccs_f denotes the amount of CO_2 that is not directly utilized but is compressed and then sequestered. From Fig. 12, it can be observed that during the time intervals of 5:00 to 7:00 and 19:00 to 23:00, there is an increase in CHP generation, leading to higher carbon emissions. During these periods, the CCS captures a larger quantity of CO_2, which in turn results in increased electricity consumption. A portion of the captured CO_2 is utilized by P2G, while the remaining portion is compressed and subsequently stored through transportation. The consumption of CO_2 primarily occurs during the time intervals of 1:00 to 5:00, 9:00 to 17:00, and 22:00 to 24:00, coinciding with high renewable energy output periods, during which P2G actively consumes renewable energy.

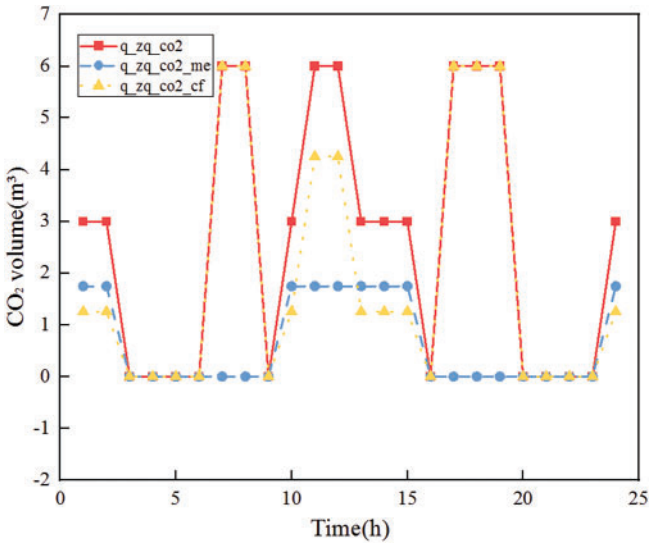

Figure 12: CO_2 traces in BG digester in case 4

Fig. 12 shows the CO_2 situation in the BG digester for case 4, where q_zq_co2 denotes the CO_2 produced by the BG digester; q_zq_co2_me denotes the CO_2 that is directly utilized by P2G, and q_zq_co2_cf denotes the CO_2 that is not directly utilized in the sequestration process. This is similar to the utilization of CO_2 in carbon capture power plant.

5 Conclusions

In this thesis, the framework of WP-PV-BG IES considering CCS and P2G conversion is constructed, and a collaborative optimal scheduling model considering operation cost is established. The main conclusions are obtained as follows:

(1) The proposed collaborative operation framework of BG-CCS-P2G makes full use of the natural gas produced by the BG pool. Then, it provides the CO_2 captured by the CCS device as a feedstock for the P2G plant to be converted into natural gas. This results in a 9.4% reduction in the cost of purchased gas relative to the original case. The P2G and CCS coupling energy storage systems can achieve 100% consumption of renewable energy.

(2) The coordinated optimal scheduling strategy can significantly reduce the renewable energy penalty cost and natural gas scheduling cost so that the total system operation cost can be reduced by RMB 2546.95, which has a very economical performance.

Acknowledgement: The authors sincerely acknowledge the contribution of all individuals, reviewers, and editors for their contribution towards the production of this manuscript.

Funding Statement: The authors received no specific funding for this study.

Author Contributions: The authors confirm contribution to the paper as follows: Conceptualization, Yunfei Xu and Xiaoqing Hao; methodology, Tianxing Sun and Heran Kang; software, Jianfeng Liu and Tianxing Sun; validation, Yunfei Xu, Jianfeng Liu, Tianxing Sun, Heran Kang and Xiaoqing Hao; formal analysis, Yunfei Xu and Heran Kang; investigation, Jianfeng Liu and Xiaoqing Hao; resources, Tianxing Sun and Xiaoqing Hao; writing—original draft preparation, Yunfei Xu, Jianfeng Liu and Tianxing Sun; writing—review and editing, Yunfei Xu, Heran Kang and Xiaoqing Hao; supervision, Jianfeng Liu and Xiaoqing Hao; project administration, Yunfei Xu and Xiaoqing Hao. All authors reviewed the results and approved the final version of the manuscript.

Availability of Data and Materials: The data presented in this study are available on request from the corresponding author.

Ethics Approval: Not applicable.

Conflicts of Interest: The authors declare no conflicts of interest to report regarding the present study.

Nomenclature

IES	Integrated energy systems
CCS	Carbon capture system
P2G	Power-to-gas
BG	Biogas
CHP	Combined heat and power
WP	Wind power
PV	Photovoltaic
ES	Energy storage
EL	Electrolyser
GB	Gas boiler

EB	Electric boiler
EES	Electric energy system

References

1. Yang P, Jiang H, Liu C, Kang L, Wang C. Coordinated optimization scheduling operation of integrated energy system considering demand response and carbon trading mechanism. Int J Electr Power Energy Syst. 2023;147(6):108902. doi:10.1016/j.ijepes.2022.108902.
2. Yan Q, Zhang G, Zhang Y, Yu H. Coordinated scheduling optimization of building integrated energy system with flexible load. Energy Rep. 2024;12(11):3422–36. doi:10.1016/j.egyr.2024.08.081.
3. Wang L, Ni L, Wang S, Wang J, Zhao Z, Shen H. Low-carbon economic dispatch of waste incineration power plant and biogas purification multi-energy coupling system considering power-to-gas. Energy Rep. 2025;13(3):2997–3012. doi:10.1016/j.egyr.2025.02.031.
4. Gao C, Lu H, Chen M, Chang X, Zheng C. A low-carbon optimization of integrated energy system dispatch under multi-system coupling of electricity-heat-gas-hydrogen based on stepwise carbon trading. Int J Hydrogen Energy. 2025;97(3):362–76. doi:10.1016/j.ijhydene.2024.11.055.
5. Zhang G, Wang W, Chen Z, Li R, Niu Y. Modeling and optimal dispatch of a carbon-cycle integrated energy system for low-carbon and economic operation. Energy. 2022;240:122795. doi:10.1016/j.energy.2021.122795.
6. Liao M, Liu C. Optimal coordination of electricity-P2G-gas system to facilitate renewable energy integration. Sustain Energy Grids Netw. 2025;41(4):101610. doi:10.1016/j.segan.2024.101610.
7. Xing X, Lin J, Song Y, Zhou Y, Mu S, Hu Q. Modeling and operation of the power-to-gas system for renewables integration: a review. CSEE J Power Energy Syst. 2018;4(2):168–78. doi:10.17775/cseejpes.2018.00260.
8. Wang J, Ji X, Meng X, Bai Y, Li M. Low-carbon economic dispatch of integrated energy system with carbon capture power plant and multiple utilization of hydrogen energy. Front Energy Res. 2025;12:1447858. doi:10.3389/fenrg.2024.1447858.
9. Ji Z, Kang C, Chen Q, Xia Q, Jiang C, Chen Z, et al. Low-carbon power system dispatch incorporating carbon capture power plants. IEEE Trans Power Syst. 2013;28(4):4615–23. doi:10.1109/tpwrs.2013.2274176.
10. He K, Zeng L, Yang J, Gong Y, Zhang Z, Chen K. Optimization strategy for low-carbon economy of integrated energy system considering carbon capture-two stage power-to-gas hydrogen coupling. Energies. 2024;17(13):3205. doi:10.3390/en17133205.
11. Zhang Y, Zhang P, Du S, Dong H. Economic optimal scheduling of integrated energy system considering wind-solar uncertainty and power to gas and carbon capture and storage. Energies. 2024;17(11):2770. doi:10.3390/en17112770.
12. He L, Lu Z, Zhang J, Geng L, Zhao H, Li X. Low-carbon economic dispatch for electricity and natural gas systems considering carbon capture systems and power-to-gas. Appl Energy. 2018;224(4):357–70. doi:10.1016/j.apenergy.2018.04.119.
13. Sun S, Xing J, Cheng Y, Yu P, Wang Y, Yang S, et al. Optimal scheduling of integrated energy system based on carbon capture-power to gas combined low-carbon operation. Processes. 2025;13(2):540. doi:10.3390/pr13020540.
14. Wang Y, Gao S, Jia W, Ding T, Zhou Z, Wang Z. Data-driven distributionally robust economic dispatch for park integrated energy systems with coordination of carbon capture and storage devices and combined heat and power plants. IET Renew Power Gener. 2022;16(12):2617–29. doi:10.1049/rpg2.12436.
15. Fen Z, Lv L, Xu L. A day-ahead and real-time two-stage optimal scheduling model for a full renewable energy system based on energy hubs-marsh-wind-light. Power Syst Technol. 2019;43(9):3101–9. (In Chinese). doi:10.13335/j.1000-3673.pst.2019.0596.
16. Ghaem Sigarchian S, Paleta R, Malmquist A, Pina A. Feasibility study of using a biogas engine as backup in a decentralized hybrid (PV/wind/battery) power generation system—case study Kenya. Energy. 2015;90(2):1830–41. doi:10.1016/j.energy.2015.07.008.
17. Tan H, Yan W, Wang H. Optimal scheduling model of marsh-wind-light isolated micro-energy network based on building thermal energy flow analysis. Power Syst Technol. 2020;44(7):2483–91. (In Chinese). doi:10.13335/j.1000-3673.pst.2019.2434.

18. Rahman MM, Hasan MM, Paatero JV, Lahdelma R. Hybrid application of biogas and solar resources to fulfill household energy needs: a potentially viable option in rural areas of developing countries. Renew Energy. 2014;68:35–45. doi:10.1016/j.renene.2014.01.030.
19. Zhou B, Xu D, Li C, Chung CY, Cao Y, Chan KW, et al. Optimal scheduling of biogas-solar–wind renewable portfolio for multicarrier energy supplies. IEEE Trans Power Syst. 2018;33(6):6229–39. doi:10.1109/TPWRS.2018.2833496.
20. Zhang S, Gu W, Zhang XP, Lu H, Yu R, Qiu H, et al. Dynamic modeling and simulation of integrated electricity and gas systems. IEEE Trans Smart Grid. 2023;14(2):1011–26. doi:10.1109/tsg.2022.3203485.
21. Zhang M, Yu S, Li H. Inter-zone optimal scheduling of rural wind-biomass-hydrogen integrated energy system. Energies. 2023;16(17):6202. doi:10.3390/en16176202.
22. Qin M, Yang Y, Chen S, Xu Q. Bi-level optimization model of integrated biogas energy system considering the thermal comfort of heat customers and the price fluctuation of natural gas. Int J Electr Power Energy Syst. 2023;151(2):109168. doi:10.1016/j.ijepes.2023.109168.
23. Chen W, Chang X, Li J. A day-ahead optimal scheduling model of an integrated energy system for a facility agricultural-industrial park. IET Energy Syst Integr. 2023;5(3):261–74. doi:10.1049/esi2.12101.